

## PROSPECTS FOR REDSHIFTED 21-CM OBSERVATIONS OF QUASAR H II REGIONS

J. STUART B. WYITHE<sup>1</sup>, ABRAHAM LOEB<sup>2</sup>, DAVID G. BARNES<sup>1</sup>  
 swyithe@physics.unimelb.edu.au; aloeb@cfa.harvard.edu; dbarnes@physics.unimelb.edu.au  
*Draft version December 2, 2018*

## ABSTRACT

The introduction of low-frequency radio arrays over the coming decade is expected to revolutionize the study of the reionization epoch. Observation of the contrast in redshifted 21cm emission between a large H II region and the surrounding neutral IGM will be the simplest and most easily interpreted signature. We assess the sensitivity of three generations of planned low-frequency arrays to quasar-generated H II regions. We find that an instrument like the planned *Mileura Widefield Array Low-Frequency Demonstrator* (LFD) will be able to obtain good signal to noise on H II regions around the most luminous quasars, and determine some gross geometric properties, e.g. whether the H II region is spherical or conical. A hypothetical follow-up instrument with 10 times the collecting area of the LFD (MWA-5000) will be capable of mapping the detailed geometry of H II regions, while SKA will be capable of detecting very narrow spectral features as well as the sharpness of the H II region boundary. The SKA will most likely be limited by irreducible noise from fluctuations in the IGM itself. The MWA-5000 (and even the LFD under favorable circumstances) will discover serendipitous H II regions in widefield observations. We estimate the number of H II regions which are expected to be generated by quasars based on the observed number counts of quasars at  $z \sim 6$ . Assuming a late reionization at  $z \sim 6$  we find that there should be several tens of quasar H II regions larger than 4Mpc at  $z \sim 6 - 8$  per field of view. Identification of H II regions in forthcoming 21cm surveys can guide a search for bright galaxies in the middle of these regions. Most of the discovered galaxies would be the massive hosts of dormant quasars that left behind fossil H II cavities that persisted long after the quasar emission ended, owing to the long recombination time of intergalactic hydrogen. A snap-shot survey of candidate H II regions selected in redshifted 21cm image cubes may prove to be the most efficient method for finding very high redshift quasars and galaxies.

*Subject headings:* cosmology: theory - galaxies: formation

## 1. INTRODUCTION

The Gunn-Peterson (1965, hereafter GP) troughs in the spectra of the most distant quasars at redshifts  $z \sim 6.3-6.4$  (Djorgovski et al. 2001; Becker et al. 2001; Fan et al. 2004) hint that the reionization of cosmic hydrogen was completed only a billion years after the big bang. Unfortunately, the troughs only set a lower limit of  $\sim 10^{-3}$  on the volume averaged neutral fraction (Fan et al. 2001; White et al. 2003). This leaves open the question of whether reionization was completed only at  $z \sim 6$  so that the GP trough is due to a significantly neutral IGM, or whether it is only a residual neutral fraction left over from reionization at an earlier epoch that is responsible for the observed Ly $\alpha$  absorption. We can start to answer this question by noting that the sizes of H II regions generated by luminous quasars (Madau & Rees 2000; Cen & Haiman 2000; Barkana & Loeb 2003) at  $z > 6$  imply a neutral fraction that is of order unity at that time (Wyithe & Loeb 2004a; Wyithe, Loeb & Carilli 2005). In addition Messinger & Haiman (2004) analyzed SDSS 1030+0524 and found that the shape of the absorption spectrum near the edge of the H II region requires a large neutral fraction. These findings appear in conflict with evidence presented by the WMAP satellite in favor of early reionization (Kogut et al. 2003; Spergel et al. 2003). Indeed, if reionization ended only at  $z \sim 6$ , then more extended reionization scenarios

involving a massive early population of stars may be required (Wyithe & Loeb 2003a; Cen 2003; Furlanetto & Loeb 2005).

The large optical depth for Ly $\alpha$  absorption in a neutral intergalactic medium (IGM) limits its effectiveness in probing reionization at redshifts beyond  $z \sim 6$ . A better probe of the reionization history involves the redshifted 21cm emission from neutral hydrogen in the IGM. Various experiments are planned to measure this emission and are summarized in §2. Several probes of the reionization epoch in redshifted 21cm emission have been suggested. These include observation of the emission as a function of redshift averaged over a large area of the sky. This provides a direct probe of the evolution in the neutral fraction of the IGM, the so-called global step (Shaver, Windhorst, Madau & de Bruyn 1999; Gnedin & Shaver 2004). A more powerful probe will be provided by observation of the power-spectrum of fluctuations together with its evolution with redshift. This observation would trace the evolution of neutral gas with redshift as well as the topology of the reionization process (e.g. Tozzi, Madau, Meiksin & Rees 2000; Furlanetto, Hernquist & Zaldarriaga 2004; Loeb & Zaldarriaga 2004; Barkana & Loeb 2005a,b,c). Finally observation of individual H II regions will probe quasar physics as well as the evolution of the neutral gas (Wyithe & Loeb 2004b; Kohler, Gnedin, Miralda-Escude & Shaver 2005). Kohler et al. (2005) have generated syn-

<sup>1</sup> University of Melbourne, Parkville, Victoria, Australia

<sup>2</sup> Astronomy department, Harvard University, 60 Garden St., Cambridge, MA 02138

thetic spectra using cosmological simulations. They conclude that quasar H II regions will provide the most prominent individual cosmological signals. In this paper we concentrate on the signature of individual quasar H II regions with emphasis on the capabilities of planned telescopes.

While most discussion of reionization signatures in redshifted 21cm radiation has centered on indirect probes of the earliest galaxies through their statistical effect on the IGM, the detection of H II regions will provide specific sites where high redshift galaxies and quasars must be present. The absence of neutral hydrogen within H II regions means that these are also sites where the sources can be studied with less interference from rest-frame Ly $\alpha$  absorption. Indeed for this reason Cen (2003) has suggested H II regions around known high redshift quasars as sites to search for high-redshift galaxies. While known high redshift galaxies are rare, the advent of low-frequency radio telescopes will enable discovery of a large number of H II regions. Some of these regions will house luminous quasars, while most will house galaxies and groups of galaxies. Targeted near to mid-IR observations of 21cm selected H II regions will help define the role of different classes of sources in the reionization of the IGM.

A radio telescope is limited in sensitivity by two separate factors. The first corresponds to its physical configuration, such as the limit on resolution (set by the largest baseline) or the flux limit that can be detected over a reasonable observing time at the required resolution (set by the collecting area). Second, the theoretical limits based on the telescope dimensions may not be realized due to difficulties in achieving a perfect calibration, or due to problems introduced by foregrounds and the ionosphere. There has been significant discussion in the literature regarding foregrounds. While the fluctuations due to foregrounds are orders of magnitude larger than the reionization signal (e.g. di Matteo, Perna, Abel & Rees 2002; Oh & Mack 2003), the foreground spectra are anticipated to be smooth. Since the reionization signatures include fluctuations in frequency as well as angle, they can be removed through continuum subtraction (e.g. Gnedin & Shaver 2004; Wang, Tegmark, Santos & Knox 2005) or removed using the differences in symmetry from power-spectra analyses (Morales & Hewitt 2004; Zaldarriaga et al. 2004). In this paper we concentrate on the theoretical limitations of planned 21cm instruments. The practical difficulties introduced by calibration and foreground removal etc. need to be addressed by full simulations of interferometric observations, and ultimately with early data sets from new facilities.

The paper is organized as follows. We begin in §2 by summarizing the design properties of low frequency telescopes that are currently being planned or constructed. We then discuss the response of a synthesis array to the 21cm signature of an H II region in the presence of fluctuating background emission from density inhomogeneities in the IGM (§3). The sizes of known quasar H II regions, and our models for quasar H II regions are described in §4 and §5. Mock observations are then presented in §6 to enable assessment of the performance that is possible from

the planned instruments. In §7 we estimate the number of H II regions expected per field of view. We then discuss some science goals in §8 before summarizing our conclusions in §9.

## 2. PLANNED LOW FREQUENCY TELESCOPES

A variety of instruments capable of detecting emission from neutral gas in the high redshift IGM are planned or are under construction. Interferometric arrays currently under construction include the Primeval Structure Telescope<sup>3</sup> (PAST), the Low Frequency Array<sup>4</sup> (LOFAR) and a re-fitting of the VLA with low-frequency (200MHz) receivers (L. Greenhill et al). Of these, the low frequency VLA will have the smallest collecting area. However this system has been especially designed with observation of H II regions around known high redshift quasars in mind. Conversely the PAST experiment is designed to perform a deep observation of the north Celestial Pole with an aim of detecting the power-spectrum of 21cm fluctuations. In its initial form PAST will not have a pointable primary beam and so is less suited to observing known H II regions. The LOFAR telescope will consist of phased arrays of cross-dipoles grouped in a large number of stations or tiles. Each tile has a large primary beam covering many square degrees. LOFAR will be capable of operating with pointed observations over a wide band-pass at redshifts from 5-20. While the northern European site on which LOFAR is being built is not an ideal radio environment, LOFAR will be complementary to the planned Mileura Widefield Array<sup>5</sup> which we describe below.

The Mileura Wide-field Array (MWA) is a collaboration of the Massachusetts Institute of Technology, Harvard-Smithsonian Center for Astrophysics, an Australian University Consortium led by Melbourne and the Australian National Universities, the Australia Telescope National Facility, and the Western Australian government. This paper is concerned only with observations using the low-frequency portion of the planned MWA (the MWA-Low Frequency Demonstrator) which we simply refer to as the LFD. The telescope will be located at the Mileura radio quiet site in Western Australia, and the low frequency portion of the array would consist of 500 tiles each containing 16 cross dipoles which operate over the range 80-300MHz. The tiles would be spread to cover baselines of up to  $\sim$  2km. In collecting area the LFD would be comparable to the VLA. However the correlator/receiver system will be able to handle a much larger number of channels than will be available on the low frequency VLA. A hypothetical follow up to the LFD would comprise 10 times the collecting area of the LFD, with baselines of  $\sim$  10s to 100s of kilometers (we refer to this as MWA-5000). The physical attributes of the MWA-5000 would be comparable to LOFAR as an instrument for study of reionization. Finally a Square Kilometer Array (SKA) would become the next generation radio telescope. An SKA would have the collecting area of  $\sim$  10 times the MWA-5000, with baselines up to  $\sim$  1000km or greater. In this paper we concentrate our discussion on the capabilities of the LFD, MWA-5000 and SKA. However discussion of the LFD is also broadly

<sup>3</sup> <http://web.phys.cmu.edu/past/>

<sup>4</sup> <http://www.lofar.org/>

<sup>5</sup> <http://web.haystack.mit.edu/arrays/MWA/>

applicable to the low-frequency VLA, while the discussion of the MWA-5000 could be applied to LOFAR.

### 3. TELESCOPE RESPONSE

In this section we discuss the response of a phased array to the brightness temperature contrast introduced by an H II region. Assuming that calibration can be performed ideally, and that foreground subtraction is perfect, the root-mean-square fluctuations in brightness temperature are given by the radiometer equation

$$\langle \Delta T^2 \rangle^{1/2} = \frac{C \lambda^2 T_{\text{sys}}}{A_{\text{tot}} \Omega_b \sqrt{t_{\text{int}} \Delta \nu}}, \quad (1)$$

where  $\lambda$  is the wavelength,  $T_{\text{sys}}$  is the system temperature,  $A_{\text{tot}}$  the collecting area,  $\Omega_b$  the effective solid angle of the synthesized beam in radians,  $t_{\text{int}}$  is the integration time,  $\Delta \nu$  is the size of the frequency bin, and  $C$  is a constant that describes the overall efficiency of the telescope. We optimistically adopt  $C = 1$  in this paper. In units relevant for upcoming telescopes, and at  $\nu = 200\text{MHz}$  we find

$$\Delta T = 7.5 \left( \frac{1.97}{C_{\text{beam}}} \right) \text{mK} \left( \frac{A}{A_{\text{LFD}}} \right)^{-1} \times \left( \frac{\Delta \nu}{1\text{MHz}} \right)^{-1/2} \left( \frac{t_{\text{int}}}{100\text{hr}} \right)^{-1/2} \left( \frac{\Delta \theta_{\text{beam}}}{5'} \right)^{-2}. \quad (2)$$

Here  $A_{\text{LFD}}$  is the collecting area of a phased array consisting of 500 tiles each with 16 cross-dipoles [the effective collecting area of an LFD tile with  $4 \times 4$  cross-dipole array with 1.07m spacing is  $\sim 17 - 19\text{m}^2$  between 100 and 200MHz (B. Correy, private communication)]. The system temperature at 200MHz will be dominated by the sky and has a value  $T_{\text{sys}} \sim 250\text{K}$ . The frequency range over which the signal is smoothed is  $\Delta \nu$  and  $\Delta \theta_{\text{beam}}$  is the size of the synthesized beam in arc-minutes. The beam size  $\Delta \theta_{\text{beam}}$  can be interpreted as the radius of a hypothetical top-hat beam, or as the variance of a hypothetical Gaussian beam. The corresponding values of the constant  $C_{\text{beam}}$  are 1.97 and 1 respectively.

Noise from the telescope is not the only form of confusion. The density fluctuations in the IGM also produce a form of random noise relative to the detection of H II regions. Of course these fluctuations do not reduce with observing time. At times where the neutral fraction is near unity, and on large enough scales the power-spectrum of emission from density fluctuations may be calculated directly from the linear power-spectrum of primordial fluctuations. The power-spectrum is spherically symmetric in space, and may be approximated by a power-law with  $\langle \Delta T^2 \rangle^{1/2} \propto \theta_{\text{beam}}^{-1/3}$  (Furlanetto & Briggs 2004). The normalization depends on the details of the frequency smoothing scale and on the neutral fraction etc. We take the fiducial value of 3mK at  $10'$  for a smoothing of 5MHz (Furlanetto & Briggs 2004). The resulting power-spectrum is shown in Figure 1. While telescope noise is spread across the entire image cube, fluctuations from the cosmic web are present only outside the ionized regions. If the neutral fraction is near unity, then the contrast of the H II region will be much larger than the variance due to the cosmic web. Therefore if the goal is to measure the properties of the H II region, then the benefit of increasing the integration time becomes small once the noise reaches the level of

the fluctuations in the IGM emission. Optimal use of the telescope for observing H II regions therefore calls for integration times and resolutions that result in instrumental noise that is near or just below the level of variance due to the cosmic web.

For a given telescope and synthesized beam size, the minimum integration time necessary for the observation of an H II region is therefore set by the requirement that the noise be smaller than both half the maximum contrast, which is 11mK at  $z = 6.5$  (plotted as the horizontal line in Figure 1), and the fluctuations in the IGM surrounding the H II region. In addition the maximum beam size is set by the requirement that the resolution be smaller than the feature being observed. A spherical H II region at  $z \sim 6.5$  of radius 5Mpc subtends an angular radius of  $\sim 15'$  (half of which is plotted as the vertical line in Figure 1). The shaded region in Figure 1 shows the region bounded from above by variance in emission from the IGM, and from the right by resolution requirements. The parameters describing the observation of an H II region should place the noise inside, but near the top of this shaded area.

For comparison with these requirements we overplot the sensitivity of different telescopes in Figure 1. The ideal root-mean-square noise is plotted (sets of curves from right to left) for the LFD, for the MWA-5000 (with  $A_{\text{MWA-5000}} = 10A_{\text{LFD}}$ ), and for the SKA (with  $A_{\text{SKA}} = 100A_{\text{LFD}}$ ). The left and right panels represent 100 and 1000 hour integrations respectively. Each set of curves shows the instrumental noise corresponding to 4, 2, 1 and 0.5MHz smoothing (thin lines left to right). In each case the thick lines in Figure 1 show the noise as a function of synthesized beam size where the scale of the frequency smoothing is chosen to match the physical scale of the beam at the redshift of the signal. The noise behaves as  $(\Delta \theta_{\text{beam}})^{-3}$  rather than  $(\Delta \theta_{\text{beam}})^{-2}$  in this case.

The telescopes described in the previous section therefore meet the requirements for observation of H II regions over long integrations, as may be seen by inspecting Figure 1. Of course Figure 1 describes the most optimistic case, as the contrast will be lower than 22mK if the IGM is partially ionized. Moreover the integration time should be sufficiently long that the contrast is measured at a signal-to-noise significantly in excess of unity. Furthermore, for a spherical H II region the beam-size should be much smaller than the angular extent of the H II region otherwise the contrast is reduced due to dilution of the signal. Similarly, if the spectral resolution corresponds to a size in the Hubble flow that is not smaller than the extent of the H II region, then the contrast will be reduced due to dilution of the signal during smoothing in frequency. Note that it is *cheaper* in terms of telescope time to gain resolution along the line-of-sight than perpendicular to the line-of-sight.

The contrasts in Figure 1 and the remainder of this paper assume a neutral fraction of unity. However to relate the results in this paper to a neutral fraction that is smaller than unity, the integration times discussed in this paper should be increased by a factor of  $x_{\text{HI}}^{-2}$ . In addition, as the neutral fraction drops towards the end of reionization, the variance of IGM fluctuations can rise due to the appearance of ionized regions. This variance will swamp the signal of individual H II regions. Our simulations therefore correspond to the IGM before it has been substantially

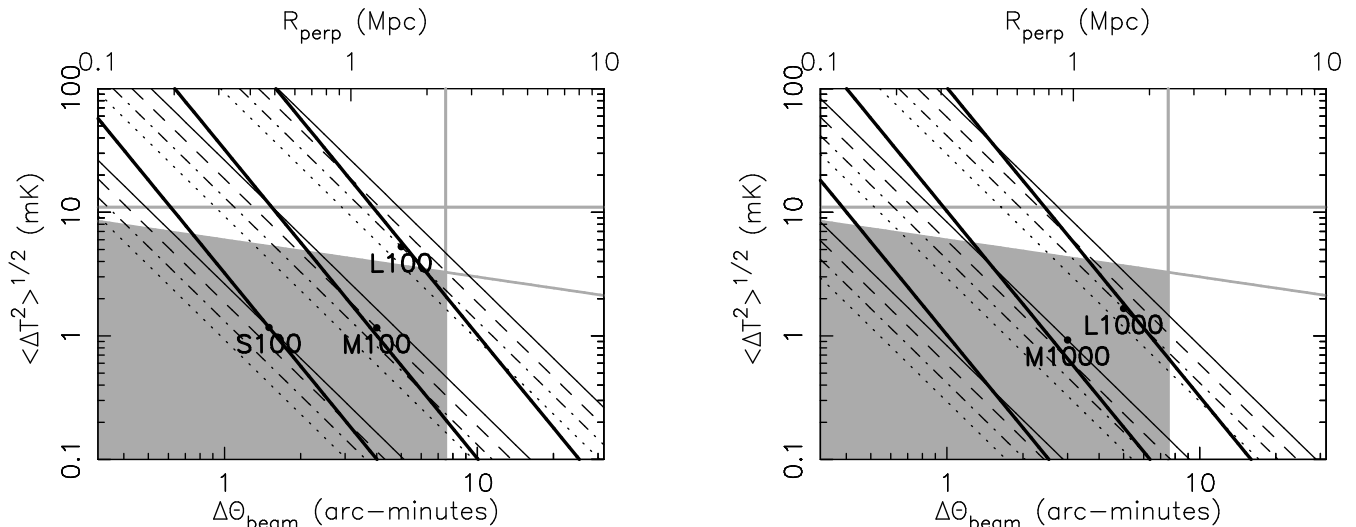


FIG. 1.— Response of different low-frequency telescopes relative to the expected signal of H II regions. The shaded region is bounded from the right by half of the size of a 5Mpc HII region, and from above by the variance in brightness temperature due to IGM density fluctuations smoothed on the scale shown and averaged in a 0.5MHz band pass. The horizontal grey line at 11mK corresponds to half of the 22mK maximum contrast between an H II region and the surrounding neutral IGM at  $z = 6.5$ . The telescope sensitivity should lie within the shaded region. The sets of dark lines show the rms noise evaluated from the radiometer equation as a function of Gaussian beam size for 0.5, 1, 2 and 4MHz bins (right to left), and for a frequency bin size that matches the physical scale of the beam (thick line). The three sets of lines correspond to a collecting area of the LFD, MWA-5000 and SKA (right to left). The left and right panels are for a 100hr and a 1000hr integration respectively. The labels L100 and L1000 show the points corresponding to the LFD with 100 and 1000 hour integrations respectively (Figure 4), while the labels M100 and M1000 show the points corresponding to the MWA-5000 with 100 and 1000 hour integrations (Figures 4 and 5). The label S100 corresponds to the SKA with a 100 hour integration (Figure 7).

TABLE 1  
PROPERTIES OF  $z > 6$  QUASARS. RADII  $R$  ARE QUOTED IN MPC.

Source	$M_{1450}$	$z$	$z_{GP}$	$z_{\text{host}} - z_{GP}$	$R \pm \sigma_R$
J1148+5251	-27.82 <sup>a</sup>	$6.419 \pm 0.001^b$	$6.325 \pm 0.02^c$	$0.09 \pm 0.02$	$4.89 \pm 1.09$
J1030+0524	-27.15 <sup>d</sup>	$6.311 \pm 0.005^g$	$6.178 \pm 0.005^c$	$0.133 \pm 0.007$	$7.50 \pm 0.39$
J1048+4637	-27.55 <sup>a</sup>	$6.203 \pm 0.005^g$	$6.16 \pm 0.03^a$	$0.04 \pm 0.03$	$2.34 \pm 1.76$
J1623+3112	-26.67 <sup>e</sup>	$6.22 \pm 0.03^e$	$6.16 \pm 0.03^e$	$0.08 \pm 0.04$	$4.65 \pm 1.74$
J1602+4228	-26.82 <sup>e</sup>	$6.07 \pm 0.03^e$	$5.95 \pm 0.03^e$	$0.12 \pm 0.04$	$7.36 \pm 2.45$
J1630+4012	-26.11 <sup>a</sup>	$6.065 \pm 0.005^g$	$5.98 \pm 0.03^a$	$0.085 \pm 0.03$	$5.22 \pm 1.84$
J1306+0356	-27.19 <sup>d</sup>	$5.99 \pm 0.02^f$	$5.90 \pm 0.03^d$	$0.09 \pm 0.04$	$5.68 \pm 2.52$

<sup>a</sup>Fan et al. (2003); <sup>b</sup>Walter et al. (2003); <sup>c</sup>Bertoldi et al. (2003); <sup>e</sup>White et al. (2003)

<sup>d</sup>Fan et al. (2001); <sup>e</sup>Fan et al. (2004); <sup>f</sup>Maiolino et al. (2003); <sup>g</sup>Iwamuro et al. (2004)

reionized.

#### 4. PROPERTIES OF THE KNOWN $z > 6$ QUASARS AND PUTATIVE H II REGIONS

The Sloan Digital Sky Survey (*SDSS*) has discovered seven quasars at  $z \geq 6$  (Fan et al. 2001;2003;2004). These quasars are listed in Table 1. Column 2 lists the ultraviolet AB magnitudes. Column 3 lists the source redshifts and column 4 lists the redshift for the onset of the GP absorption (see below). Column 5 lists the difference between the host galaxy redshift (see below) and the GP redshift, while column 6 gives the corresponding size ( $R$ ) in physical Mpc of the H II region. The typical size for H II regions around luminous quasars at  $z \sim 6$  is  $R \sim 5$ Mpc. In this paper we concentrate on investigating the observability of H II regions of this size.

#### 5. MODELS OF QUASAR H II REGIONS

Given a line-of-sight ionizing photon emission rate of  $\dot{N}/4\pi$  photons per second per steradian and a uniform IGM, the line-of-sight extent of a quasar's H II region (from quasar to the *front* of the region) observed at time  $t$  is (White et al. 2003)

$$R = 4\text{Mpc} \left[ \frac{\dot{N}}{10^{57} x_{\text{HI}}^{-1} \frac{t_{\text{age}}}{10^7 \text{yr}}} \left( \frac{1+z}{7.5} \right)^{-3} \right]^{1/3}. \quad (3)$$

Here  $x_{\text{HI}}$  is the neutral fraction, and

$$t_{\text{age}} = t - R(t_{\text{age}})/c \quad (4)$$

is the age of the quasar corresponding to the time when photons that reach  $R$  at time  $t$  were emitted. Using this relation between proper and retarded time we can compute the observed shape of an H II region given an intrinsic shape (Wyithe & Loeb 2004b; Yu 2004). Relativistically expanding H II regions appear beamed at the front and

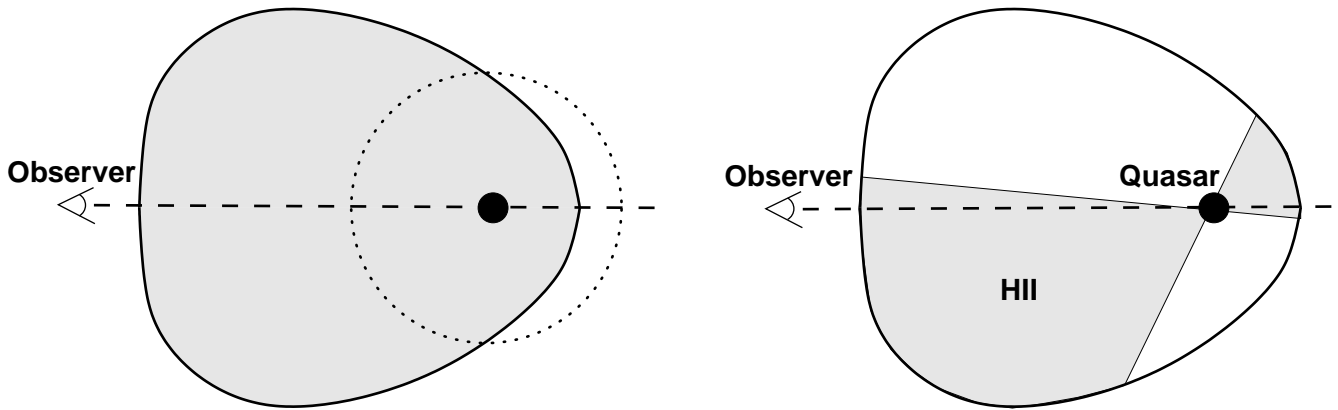


FIG. 2.— A schematic illustration of the observed H II region geometry. The outer egg shaped boundary represents the shape of the surface of a relativistically expanding spherical H II region as seen by an observer. The dotted circle in the left panel shows the intrinsic size of the spherical H II region at a time  $t_{\text{age}}$  that is  $R/c$  prior to the observation (see Wyithe & Loeb 2004b). In the right panel we show an example of a bi-conical H II region. Here the boundary of the 21cm emission is shaped by the intersection of the equal observing-time surface with the ionization cones of the quasar (shaded). The symmetry axis of a conical H II region may be misaligned with the line-of-sight (dashed) as in the case illustrated on the right.

shortened at the back, an effect that is shown schematically in Figure 2. While the expansion velocity is not explicit in the formalism, it is implicit in the specification of the observables  $R$  and  $\dot{N}$  through equation (3).

In this paper we consider two examples for the intrinsic shape of the H II region. First we consider an intrinsically spherical H II region of radius 5Mpc. While a spherical H II region has traditionally been assumed, evidence for large obscuring dusty tori surrounding quasars may imply that the geometry of the H II region is bi-conical. Indeed there is evidence for bi-conical ionization and outflows in some AGN (e.g. Tadhunter & Tsvetanov 1989; Storchi-Bergmann, Wilson & Baldwin 1992; Grimes, Kriss & Espey 1999). Therefore as our second example we consider a cone of length 5Mpc with an opening angle of  $\pi/3$  radians. This cone is oriented at various angles relative to the line-of-sight. We assume a neutral fraction of unity ( $x_{\text{HI}} = 1$ ), and  $\dot{N} = 10^{57}$  which is typical of known luminous high redshift quasars.

## 6. SIMULATED OBSERVATIONS OF H II REGIONS

To simulate the observation of a quasar H II region we embed the simple H II regions described above into a neutral IGM with density fluctuations, add telescope noise to the resulting pixelized image cube and then smooth the result to a given synthesized beam size and frequency resolution in order to approximate the response of a synthesis array to the H II region.

Our simulations are generated at a resolution much higher than the observations in both frequency and angle. We start by adding fluctuations in brightness temperature due to density fluctuations in the IGM (at  $z = 6.5$ ). The fluctuations are added by generating a realization of a pixelized density field described by an isotropic power-spectrum, which on the scales of interest may be approximated by the form  $\langle \Delta T^2 \rangle^{1/2} \propto \Delta \theta^{-0.3}$  (Furlanetto & Briggs 2004). We smooth this field using a  $10'$  top-hat beam and a 0.5MHz top-hat frequency filter. The amplitudes of the pixelized density field are then scaled so that the variance of the smoothed density field is 3mK (Furlanetto & Briggs 2004). The H II region is then embedded

into this density field. This is achieved by determining the *observed* geometry of the H II region, and then setting the brightness temperature contrast to zero at all points inside the H II region.

To approximate the response of a synthesis array we generate pixelized noise cubes containing white noise in angular dimensions, and  $1/f$  noise in the frequency domain. The pixelized cube is smoothed by the synthesized beam (for which we assume a Gaussian) and a top-hat in frequency with width corresponding to the resolution of the observation. In this paper the beam size  $\Delta \theta_{\text{beam}}$  is defined to be the variance of the Gaussian beam. The brightness temperature contrasts of the pixelized cube are then scaled so that the resulting variance in the smoothed cube equals the value derived from the radiometer equation (2). The scaled, pixelized noise cube is then added to the cube containing the emission signature.

This procedure neglects the contribution of foregrounds. A possible scheme for removing foregrounds will be to exploit the spectral flatness of the foregrounds and perform a continuum subtraction on the spectra corresponding to each spatial pixel in the synthesized image cube. One difficulty will be the frequency dependence of polarized foregrounds, however this procedure should clean the cube of foreground contribution, and leave fluctuations in the 21cm emission that are detectable in space as well as frequency. Initial simulations suggest that this will indeed be the case (C. Johnston et al. in prep). The assumption that this cleaning can be performed efficiently is implicit in the results of this paper where image slices are shown. In addition to the image slices, we show line-of-sight spectra. These spectra are made by averaging adjacent spectra in pixels that fall within an aperture whose radius equals the size of the synthesized beam. Thus the signal to noise in these spectra is higher than expected from Figure 1 because the effective spatial resolution is  $\sim 2\Delta \theta_{\text{beam}}$ .

As discussed in § 2 there are three planned steps in the development of electronically steerable low-frequency radio telescopes capable of observing signatures of the epoch of reionization. Each step will involve an order of magni-

tude increase in the collecting area available, and allow higher resolution observations. In the remainder of this section, we show examples of the observations possible with each of these instruments.

### 6.1. Observing H II regions with the LFD

Inspection of Figure 1 shows that the root-mean-square noise falls in the shaded region for integrations longer than 100hrs and for frequency smoothing greater than 1MHz. As a demonstration, the top row of Figure 3 shows a simulated observation of a 5Mpc intrinsically spherical H II region. The integration time was 100 hours, the beam size was  $5'$ , and top-hat smoothing in frequency space was applied at 2MHz. The location of the resulting telescope noise is shown in Figure 1 by the label L100. The left-most three panels show three different slices through the image cube in frequency space. The right-most panel shows three spectra. These spectra were obtained by averaging pixels spatially within a circular aperture having the scale of the beam. The three spectra correspond to the three lines-of-sight shown by the set of circles in the third frequency slice. These circles show the size of the averaged regions for each spectrum. The left, center and right lines-of-sight are shown by the dashed, solid and dotted lines. The size of the beam is shown by the black dot at  $\theta = (-20, -20)$ . The presence of an H II region could be inferred from this data, but no information would be gleaned regarding its geometry. The relatively small contrast with respect to the background might make serendipitous discovery of H II regions difficult. On the other hand, one would have more confidence in this detection of an H II region if it were around a known high redshift quasar. In particular if the H II region is coincident with an already known quasar, then the redshift of the edge of the H II region would have a known redshift from near-IR observations (dashed vertical line in the right-hand panel).

The lower three rows show results from longer integrations of 1000 hours using a beam size of  $5'$ . The smoothing in frequency space was applied at 2MHz. The location of the resulting telescope noise is shown in Figure 1 by the label L1000. Firstly the second row repeats the observation of the sphere. The additional integration time reduces the noise to well below the contrast of the H II region. As a result the H II region is detected at high significance, and the contrast is larger due to the smaller beam size. However the size of the smoothing in frequency space 2MHz is comparable to the size of the H II region. Therefore the sharpness of the edge of the H II region cannot be determined.

The lower two rows show H II regions with conical geometry. In the 3rd row the cone is aligned with the line-of-sight, while in the bottom row the cone is oriented perpendicular to the line-of-sight. The resolution in frequency of these spectra is not sufficiently small to show the absence of ionized hydrogen at the redshift of the quasar where the cone is pointed along the line-of-sight. However in the lower-row the smaller synthesized beam provides sufficient resolution that the observation is able to see the two individual lobes of the bi-conical H II region. In addition, the averaged spectra in the 1000hr integrations show evidence for asymmetry owing to relativistic expansion in the cases of a spherical H II region, and a conical H II

region oriented along the line-of-sight (second and third rows). Thus, under favorable circumstances the LFD may already provide useful information regarding the existence, number and even geometry of H II regions.

### 6.2. Observing H II regions with the MWA-5000

While the LFD may be sufficient to detect H II regions around high redshift quasars under favorable circumstances, the MWA-5000 would be an instrument with a collecting area sufficient to reach an instrumental noise that is comparable to the cosmic web fluctuations at resolutions significantly below the size of these H II regions (see Figure 1). Here we show examples of observations of H II regions using MWA-5000 with integration times of 100 hours (Figure 4) and 1000 hours (Figure 5). In each case we show a spherical H II region (upper rows), a conical H II region oriented along the line-of-sight (second rows), a conical H II region oriented at  $\pi/4$  to the line-of-sight (third rows), and a conical H II region oriented perpendicular to the line-of-sight (bottom rows). The additional collecting area of the MWA-5000 allows observations to be made with a smaller synthesized beam, and at higher spectral resolution. For the 100 hour observation we adopt a beam size of  $4'$ , but decrease the smoothing in frequency to 1MHz, while for the 1000 hour observation we reduce the beam size to  $3'$  and use a frequency smoothing of 0.5MHz. The resulting telescope noise levels are plotted in Figure 1 using labels M100 and M1000 respectively.

With these higher resolution observations the H II regions are easily detected. Moreover the signal to noise is sufficient that the H II regions could be discovered serendipitously in MWA-5000 fields. The geometry of the individual H II regions can be determined to some degree. For example, in the 100hr integration the relativistic shortening of the back of the bubble can be seen in the spherical case, and in the case where the cone is directed along the line-of-sight. This can be seen either from the frequency slices which show a lack of H II region behind the bubble, or from the averaged spectra which show that the minimum emission is at a redshift blueward of the quasar. The synthesized maps from the 100 hr observation reveal the conical geometry where the cone is oriented away from the line-of-sight. Indeed where the cone is pointed at  $\pi/4$  to the line-of-sight the cone in front of the quasar appears larger due to relativistic beaming. Inspection of the averaged spectra also reveals the conical geometry. While the three lines-of-sight through the spherical H II region (top row) each find the same contrast, observations of a conical H II region oriented along the line-of-sight (second row) show that the central spectrum (solid line) has the higher contrast because observations from either side contain emission from neutral gas at the redshift of the quasar. If the cone is oriented at  $\pi/4$  to the line-of-sight (third row) then the conical geometry and orientation, as well as the relativistic expansion can be deduced from the relative depths of the spectra, and the redshifts where the contrast is maximized. Finally, if the cone is oriented perpendicular to the line-of-sight then the observations either side of the line-of-sight reveal the same contrast at the redshift of the quasar, while contrast along the line-of-sight is reduced.

The situation is improved still further if the integration

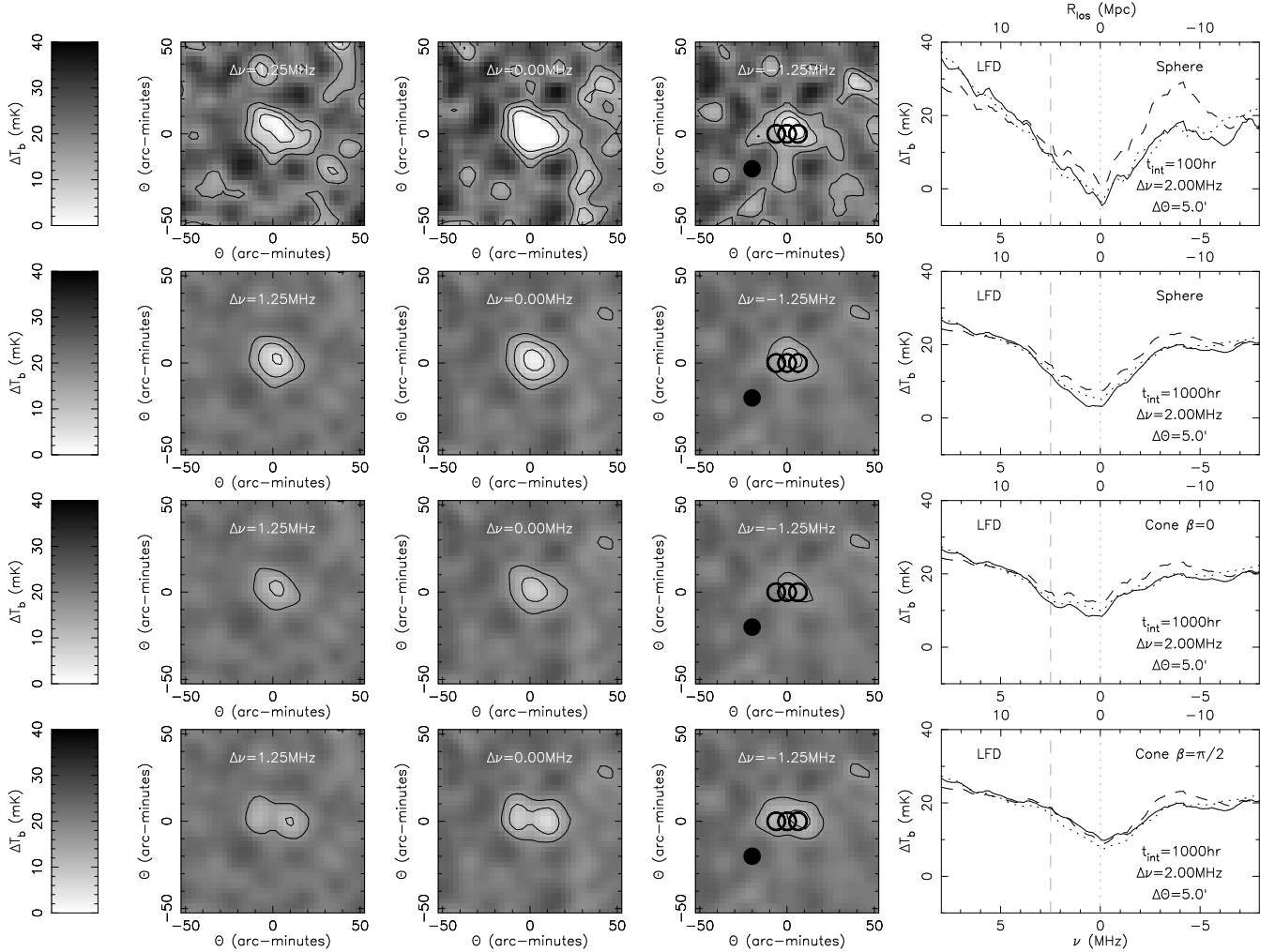


FIG. 3.— Sample maps of quasar H II regions observed with the LFD around quasars at  $z = 6.5$ . Four rows are shown. The first and second rows correspond to a 100hr and 1000hr observation of an intrinsically spherical H II region. The observations were made with a  $5'$  Gaussian beam, top-hat smoothed at 2MHz. The third and fourth rows correspond to a 1000hr integration with a  $5'$  Gaussian beam, top-hat smoothed at 2MHz of an intrinsically bi-conical H II region with an opening angle of  $\pi/3$  oriented along and perpendicular to the line-of-sight respectively. In each case three slices of the frequency cube are shown. The contours correspond to 5, 11 and 17mK. In addition, 3 smoothed spectra are shown in the right-most panel. These are obtained by integrating over pixels inside one beam radius from points along, and points  $R_{\text{cone}}/2$  left and right of the line-of-sight. The beams at these points are plotted on the third frequency slice. The dashed, solid and dotted spectra correspond to the left, center and right lines-of-sight respectively, while the dotted and dashed vertical lines show the redshifts of the quasar and the front of the H II region. The solid black dot at  $(-20, -20)$  shows the beam size.

time is increased to 1000 hours. The narrower frequency smoothing used in the longer integration allows the edge of the H II region to be better defined. The rear edge of the H II region occurs closer in redshift to the quasar, showing the time delay effect owing to the relativistic expansion. The morphologies described in the previous paragraph are more prominent in this case. For example, in the second row, where the cone is oriented along the line-of-sight, the high resolution and small frequency bin result in the observation of a peak of emission at the redshift of the quasar. This peak is the result of our idealized conical geometry. If the host galaxy produced an inner spherical H II region, this peak would be less prominent in the observations.

The most luminous quasars discovered near the end of the reionization epoch have putative H II regions of 5Mpc. These are the largest H II regions we expect to find, because quasars at higher redshift should be less luminous. How small could the quasar H II region be and still re-

main detectable by the MWA-5000? Inspection of Figure 1 suggests that in  $\sim 1000$  hours, regions of  $\sim 1$ Mpc could just be detectable; however this may be degraded by the presence of the fluctuations in the IGM. In Figure 6 we show simulated observations of intrinsically spherical H II regions with the MWA-5000. The integration time was 1000 hours. As before the left-most three panels show three different slices through the image cube in frequency space. The right-most panel shows three spectra. These spectra were obtained by averaging pixels spatially within a circular aperture having the scale of the beam. The three spectra correspond to the three lines-of-sight shown by the three circles in the third frequency slice (from left to right these spectra are shown by the dashed, solid and dotted lines). The size of the beam is also shown by the black dot at  $\theta = (-20, -20)$ . The upper two rows show H II regions of  $R = 4$ Mpc and  $R = 2$ Mpc respectively for which the luminosity of the source quasar was scaled

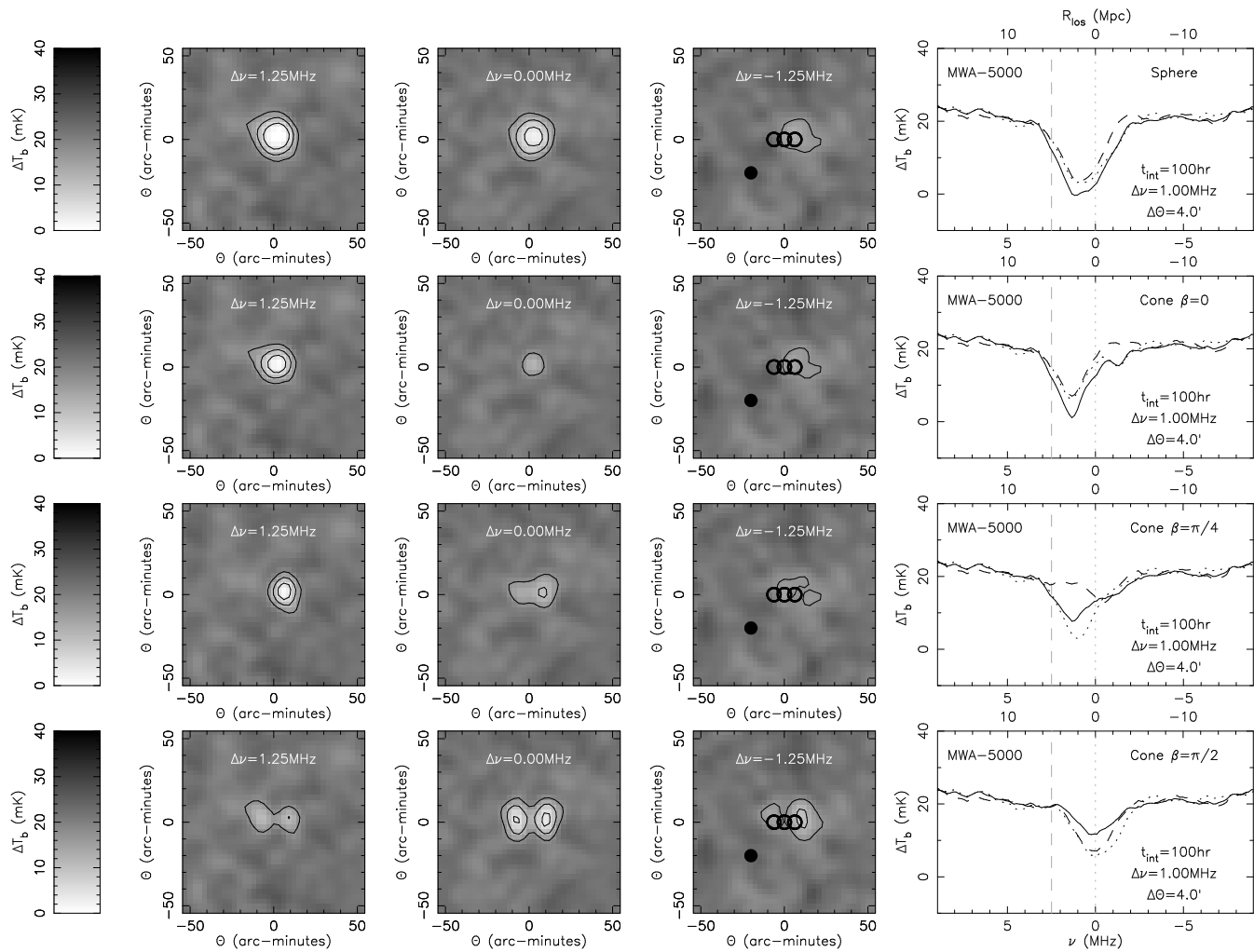


FIG. 4.— Sample maps of H II regions around quasars at  $z = 6.5$  observed with the MWA-5000 with a  $4'$  Gaussian beam and top-hat smoothed at 1MHz in a 100hr integration. Four rows are shown. The first row corresponds to observation of an intrinsically spherical H II region. The second, third and fourth rows correspond to observations of an intrinsically bi-conical H II region with an opening angle of  $\pi/3$  oriented along, at  $\pi/4$  to, and perpendicular to the line-of-sight respectively. In each case three slices of the frequency cube are shown. The contours correspond to 5, 11 and 17mK. In addition, 3 smoothed spectra are shown in the right-most panel. These are obtained by integrating over pixels inside one beam radius from points along, and points  $R_{\text{cone}}/2$  left and right of the line-of-sight. The beams at these points are plotted on the third frequency slice. The dashed, solid and dotted spectra correspond to the left, center and right lines-of-sight respectively, while the dotted and dashed vertical lines show the redshifts of the quasar and the front of the H II region. The solid black dot at  $(-20, 20)$  shows the beam size.

down in proportion to  $R^3$  relative to the previous examples. The beam size was  $3'$ , and top-hat smoothing in frequency space was applied at 0.5MHz, yielding similar spatial resolution in the directions along and perpendicular to the line-of-sight. The H II regions of this size are readily detectable with MWA-5000 at  $< 1000$  hour integration. Smaller H II regions require a synthesized beam smaller than  $3'$ . The lower two rows show H II region of  $R = 1\text{Mpc}$  and  $R = 0.5\text{Mpc}$  respectively. The luminosity of the source quasar was again scaled down in proportion to  $R^3$  relative to the previous examples. The beam size was reduced to  $2'$ , and top-hat smoothing in frequency space was applied at 0.35MHz. The  $R \lesssim 2\text{Mpc}$  H II regions will not be detectable using MWA-5000 with a 1000 hour integration.

### 6.3. Observing H II regions with the SKA

The LFD may be sufficient to detect H II regions around high redshift quasars and determine some aspects of their

geometry. If the integration time is extended to  $\sim 1000$  hours, then MWA-5000 will have sufficient sensitivity and spectral resolution to enable serendipitous discovery and detailed observation of H II regions. However the SKA would be an instrument with a collecting area sufficient to reach an instrumental noise that is smaller than the cosmic web fluctuations at resolutions much higher than the size of the H II regions (see Figure 1), allowing detailed investigation of the geometry of H II regions. Here we show examples of observations of H II regions using SKA with integration times of 100 hours (Figure 7). Following the examples for the MWA-5000 we show a spherical H II region (upper row), a conical H II region oriented along the line-of-sight (second row), a conical H II region oriented at  $\pi/4$  to the line-of-sight (third row), and a conical H II region oriented perpendicular to the line-of-sight (bottom row). The additional collecting area of the SKA allows observations to be made with a smaller synthesized beam,

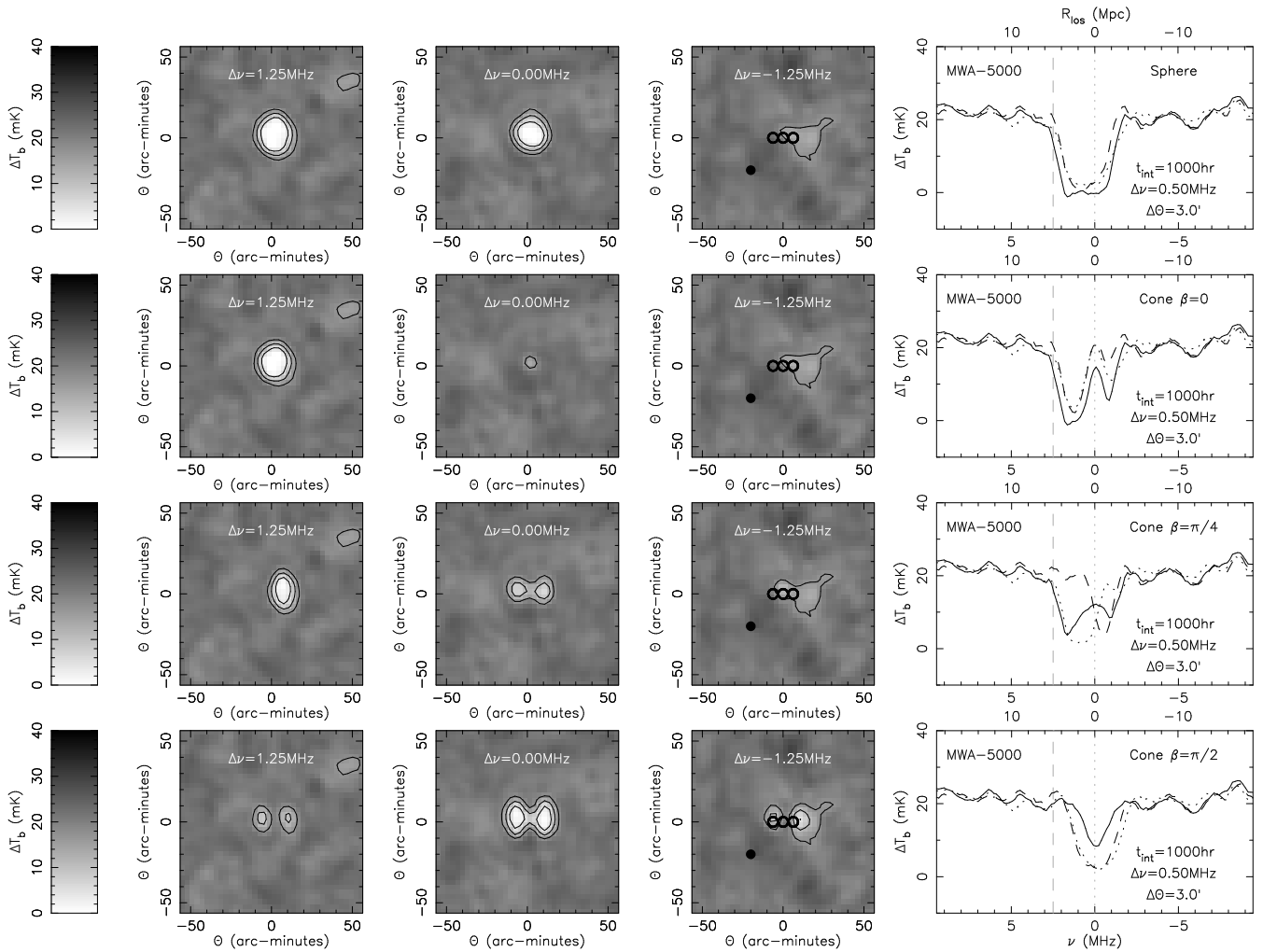


FIG. 5.— Sample maps of H II regions observed around quasars at  $z = 6.5$  with the MWA-5000 with a  $3'$  Gaussian beam and top-hat smoothed at  $0.5\text{MHz}$  in a  $1000\text{hr}$  integration. Four rows are shown. The first row corresponds to observation of an intrinsically spherical H II region. The second, third and fourth rows correspond to observations of an intrinsically bi-conical H II region with an opening angle of  $\pi/3$  oriented along, at  $\pi/4$  to, and perpendicular to the line-of-sight respectively. In each case three slices of the frequency cube are shown. The contours correspond to 5, 11 and  $17\text{mK}$ . In addition, 3 smoothed spectra are shown in the right-most panel. These are obtained by integrating over pixels inside one beam radius from points along, and points  $R_{\text{cone}}/2$  left and right of the line-of-sight. The beams at these points are plotted on the third frequency slice. The dashed, solid and dotted spectra correspond to the left, center and right lines-of-sight respectively, while the dotted and dashed vertical lines show the redshifts of the quasar and the front of the H II region. The solid black dot at  $(-20, -20)$  shows the beam size.

and at higher spectral resolution than would be possible with the MWA-5000. We reduce the beam size to  $1.5'$  and use a top-hat frequency smoothing of width  $0.25\text{MHz}$ . At  $z = 6.5$  this corresponds to comparable spatial resolution along and perpendicular to the line-of-sight. The resulting telescope noise is plotted in Figure 1 using the label S100.

As may be seen from the simulated maps in Figure 7 the SKA allows observation of fine details of the H II region geometry, including all the morphologies described for the MWA-5000 observations, but with higher signal-to-noise and at higher resolution. In particular the high spectral resolution provides an excellent detection of the sharp boundary of the H II region, allowing its location in redshift to be accurately determined. However Figure 7 demonstrates a fundamental limitation in the observation of H II regions which is imposed by the density fluctuations in the IGM. These fluctuations impose an irreducible noise in the synthesized maps for a telescope with the sensitivity

of SKA which increases in amplitude as the resolution is increased. Consequently Figure 7 approximates the best observation that can be made of an H II region.

#### 7. WHAT IS THE EXPECTED ABUNDANCE OF QUASAR H II REGIONS?

The phased array design of planned low-frequency telescopes like the MWA-5000 with a large number of stations each consisting of  $4 \times 4$  crossed dipoles provides a primary beam with a diameter of  $\sim 20$  degrees. When combined with an expected bandpass of at least  $16\text{MHz}$ , a single observation will probe a very large volume. A single field is therefore expected to contain significant numbers of luminous quasars, even given their rarity at  $z > 6$  (Fan et al. 2004). Kohler, Gnedin, Miralda-Escude & Shaver (2005) have investigated the statistics of H II regions using cosmological simulations combined with a number density of quasars using an empirical extrapolation. They found that an H II region around a low-

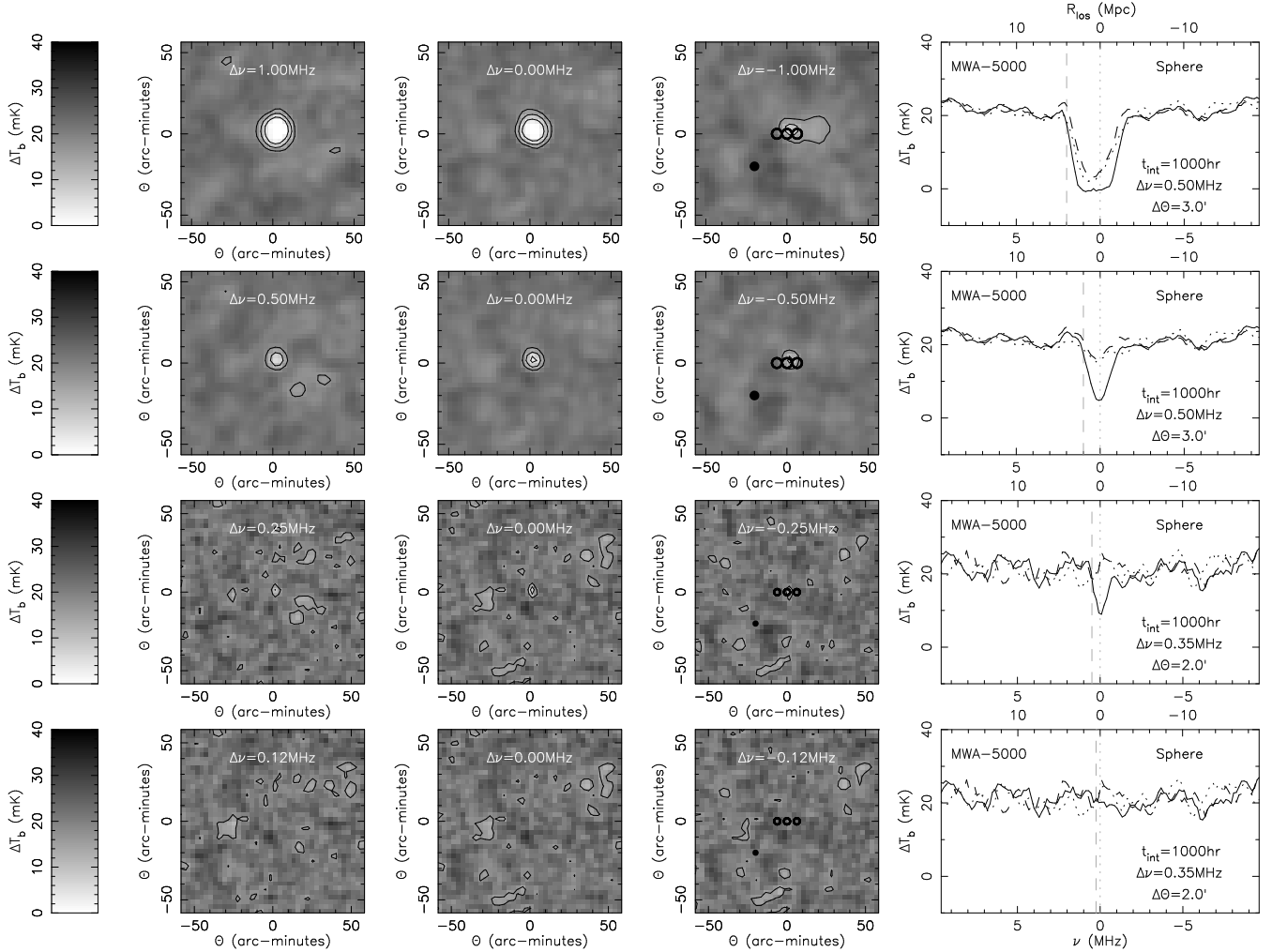


FIG. 6.— Sample maps of H II regions observed around quasars at  $z = 6.5$  with the MWA-5000 in a 1000hr integration. Four rows are shown corresponding to intrinsically spherical H II regions of size 4Mpc, 2Mpc, 1Mpc and 0.5Mpc. In the upper two rows observation was with a  $3'$  Gaussian beam, top-hat smoothed at 0.5MHz. In the lower two rows observation was with a  $2'$  Gaussian beam top-hat smoothed at 0.35MHz. In each case three slices of the frequency cube are shown. The contours correspond to 5, 11 and 17mK. In addition, 3 smoothed spectra are shown in the right-most panel. These are obtained by integrating over pixels inside one beam radius from points along, and points  $R_{\text{cone}}/2$  left and right of the line-of-sight. The beams at these points are plotted on the third frequency slice. The dashed, solid and dotted spectra correspond to the left, center and right lines-of-sight respectively, while the dotted and dashed vertical lines show the redshifts of the quasar and the front of the H II region. The solid black dot at  $(-20, -20)$  shows the beam size.

luminosity quasar should be present in each synthesized beam. Here we concentrate on H II regions around luminous quasars whose existence is known at  $z > 6$  and find the number of H II regions that we expect per primary rather than synthesized beam as this is the quantity of more interest observationally.

We estimate the number counts of quasars per 400 square-degree field in a band-pass of 16MHz as a function of B-band luminosity using two methods. First, we generate number counts using the quasar luminosity function model described in Wyithe & Loeb (2003b). Second we use an empirical extrapolation of the luminosity function found for luminous quasars at  $z \sim 6$  (Fan et al. 2004) combined with the evolution found at  $z \sim 3 - 6$  (Fan et al. 2001b) and a spectral index of  $\alpha = -0.5$ . We use equation (3) to relate the luminosity to an H II region size. The top panels of Figure 8 show the resulting number counts of H II regions of physical radius  $R$  in each of these cases, and for redshifts between  $z = 6$  and  $z = 10$ . There should

be approximately one 4Mpc H II region per field at  $z \sim 6$ , which is consistent with our finding of  $\sim 1$  quasar of the luminosity of the SDSS  $z > 6$  quasars. We estimate that there should be  $\sim 1$  quasar H II region of  $R \sim 3$ Mpc at  $z \sim 7$ ,  $\sim 1$  quasar H II region of  $R \sim 2$ Mpc at  $z \sim 8$ , and  $\sim 1$  quasar H II region of  $R \sim 1$ Mpc at  $z \sim 10$ .

However at these redshifts the recombination time is longer than the Hubble time, implying that fossil H II regions should remain in the IGM after the quasars turn off. The number of such fossil H II regions depends on the duty-cycle. For quasar lifetimes of  $\sim 10^7$  years at  $z \sim 6$  this implies a duty-cycle of  $\sim 0.01$ . Similarly, the quasar luminosity function model of Wyithe & Loeb (2003b) implies a duty-cycle of  $\sim 0.005$ . Fossil H II regions may therefore be more common than active quasars by two orders of magnitude. This results in  $\sim 100$  dormant quasar H II regions of  $R \sim 3$ Mpc at  $z \sim 7$ ,  $\sim 100$  H II regions of  $R \sim 2$ Mpc at  $z \sim 8$ , and  $\sim 100$  H II regions of  $R \sim 1$ Mpc at  $z \sim 10$ . The increase in number results in an increase

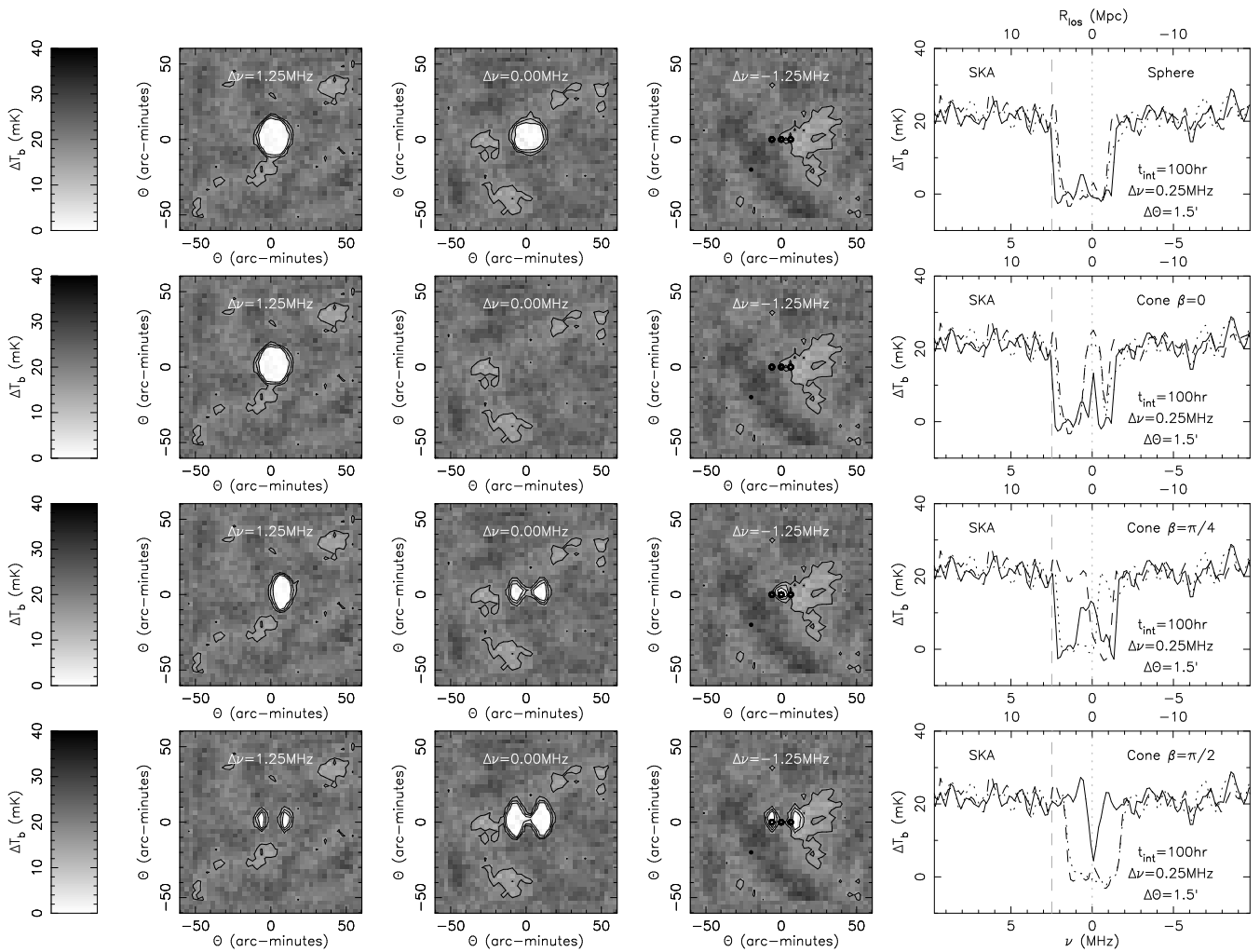


FIG. 7.— Sample maps of H II regions observed around quasars at  $z = 6.5$  using the SKA with a  $1.5'$  Gaussian beam and top-hat smoothed at  $0.25\text{MHz}$  in a  $100\text{hr}$  integration. Four rows are shown. The first row corresponds to observation of an intrinsically spherical H II region. The second, third and fourth rows correspond to observations of an intrinsically bi-conical H II region with an opening angle of  $\pi/3$  oriented along, at  $\pi/4$  to, and perpendicular to the line-of-sight. In each case three slices of the frequency cube are shown. The contours correspond to 5, 11 and  $17\text{mK}$ . In addition, 3 smoothed spectra are shown in the right-most panel. These are obtained by integrating over pixels inside one beam radius from points along, and points  $R_{\text{cone}}/2$  left and right of the line-of-sight. The beams at these points are plotted on the third frequency slice. The dashed, solid and dotted spectra correspond to the left, center and right lines-of-sight respectively, while the dotted and dashed vertical lines show the redshifts of the quasar and the front of the H II region. The solid black dot at  $(-20, -20)$  shows the beam size.

in the size of the largest H II region that might be found at a given redshift. We might therefore expect that there should be  $\sim 1$  fossil quasar H II region of  $R \sim 5\text{Mpc}$  at  $z \sim 7$ ,  $\sim 1$  quasar H II region of  $R \sim 4\text{Mpc}$  at  $z \sim 8$ , and  $\sim 1$  quasar H II region of  $R \sim 2\text{Mpc}$  at  $z \sim 10$ .

Given the numbers of H II regions that may be discovered in a single MWA-5000 field, we suggest the possibility of using near-IR followup of redshifted  $21\text{cm}$  data as an efficient means to find high redshift galaxies and quasars. In the lower panels of Figure 8 we re-plot the number counts for high redshift quasars as a function of the apparent AB magnitude at  $12500 \text{ \AA}$  (dark lines). Most regions will be fossil H II cavities from quasars that became dormant by the time of the observations. The upper axes are labeled by the corresponding integration time for the Gemini telescope<sup>6</sup>. Note that even at these high redshifts the bright quasars have  $m_{12500} \sim 20$  which is within reach of an  $8\text{m}$  class telescope in a short integration. Moreover the

redshift of any putative high redshift quasar would be approximately known (at the center of the H II region). It would therefore be practical to take a snapshot survey of an MWA-5000 field to search for unknown high-redshift quasars, even though the duty-cycle and therefore the likelihood of finding an active quasar is low.

Of course galaxies will also be present at high redshift, will generate their own H II regions, and will be found within fossil H II regions of quasars. As a function of apparent magnitude we estimate the number counts of star-burst galaxies as follows. Following Loeb, Barkana & Hernquist (2004) we find the mass of a dark matter halo corresponding to the implied luminosity for a fixed lifetime and star-formation efficiency. We have chosen sets of  $(f_{\text{star}}, t_g) = (0.1, 10^8)$  and  $(f_{\text{star}}, t_g) = (0.01, 10^7)$ . These are combinations that produce less than 1 galaxy with  $z < 20$  per 5000 square degrees, as implied by the lack of

<sup>6</sup> We used the integration time calculator for NIRI on Gemini, see <http://www.gemini.edu/sciops/instruments/instrumentITCIndex.html>

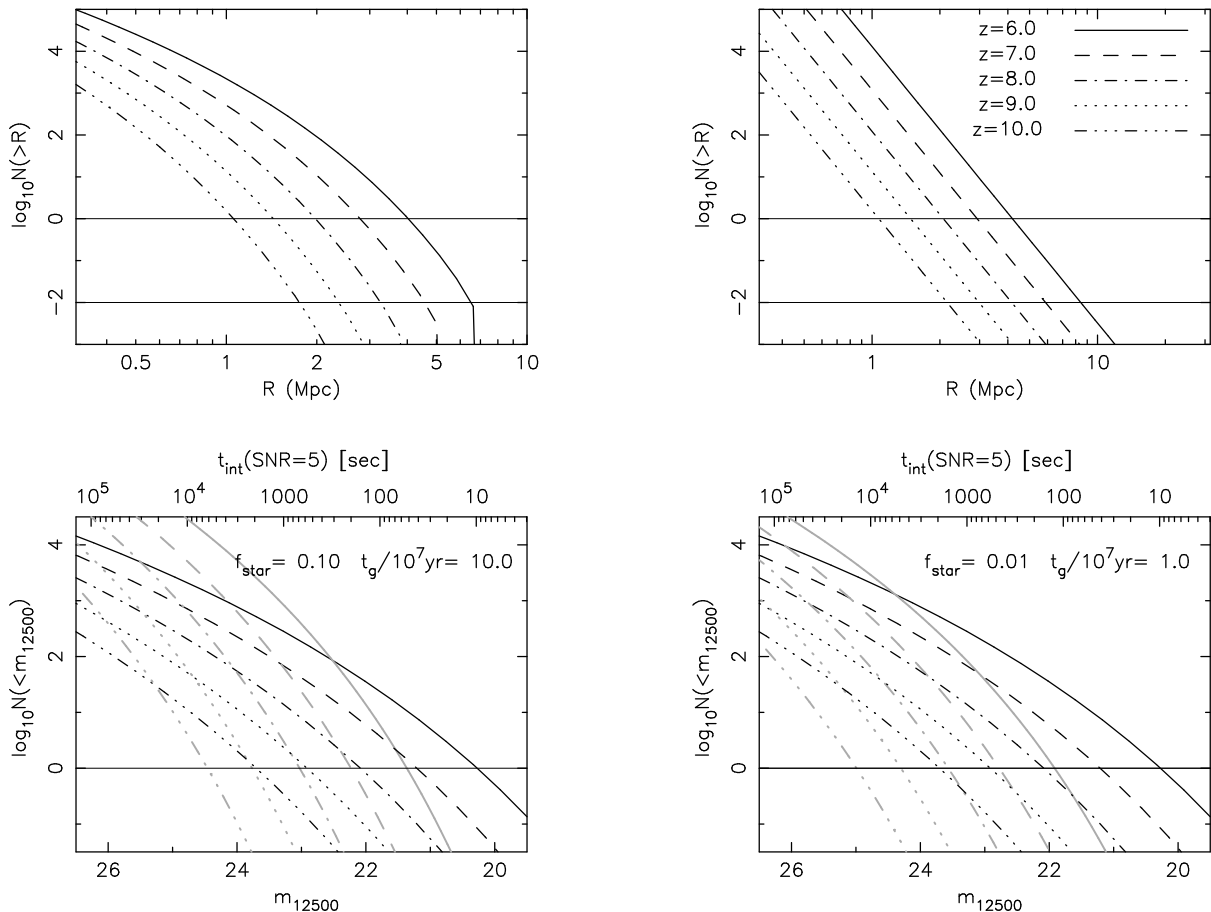


FIG. 8.— Number counts of high redshift galaxies and quasars per 400 square degree - 16MHz bandpass field. *Upper panels:* The number of quasar H II regions larger than  $R$ . We have converted from luminosity to  $R$  using equation (3). In the left panel the number counts were obtained from the model quasar luminosity function described in Wyithe & Loeb (2003b). In the right-hand panel the counts were obtained by extrapolating to high redshifts the luminosity function derived for  $z \sim 6$  quasars (Fan et al. 2004), together with the redshift evolution of quasar density (Fan et al. 2001b). Number counts are shown at redshifts between 6 and 10. The horizontal line at unity guides the eye to the largest H II region around an active quasar in the field. A second horizontal line at  $10^{-2}$  corresponds to the largest fossil H II region (around a dormant quasar) in the field assuming a duty-cycle of 1%. *Lower panels:* The dark lines show number counts of quasars (using the model luminosity function of Wyithe & Loeb 2003b) as a function of apparent AB magnitude at  $12500\text{\AA}$ . Also shown (grey lines) are the number counts of starburst galaxies assuming  $f_{\text{star}} = 0.1$ ,  $t_g = 10^8\text{yr}$  (left) and  $f_{\text{star}} = 0.01$ ,  $t_g = 10^7\text{yr}$  (right). The luminosities were computed following the prescription in Loeb et al. (2004), and the abundance from the Press-Schechter (1974) formalism. The upper axis shows an estimate of the integration time required by the Gemini Telescope (computed using the Gemini exposure time calculator). The horizontal line at unity guides the eye as to the brightest sources in the field.

such galaxies at  $z > 6$  in the SDSS. These number counts are therefore upper limits. The abundance of dark-matter halos multiplied by the duty-cycle then gives the number-counts of star-burst galaxies per MWA-5000 field which are plotted (grey lines) in the lower-panels of Figure 8 for comparison with the quasar number-counts. Bright quasars are expected to be more common than bright galaxies as would be expected from the results of the SDSS (Fan et al. 2004). The largest H II regions are therefore produced by quasars. For example, at  $z \sim 7$  we expect quasars to be more common for objects brighter than  $m_{12500} \sim 23.5$ . We expect  $\sim 100$  H II regions per field from quasars of this luminosity. However these H II regions have sizes of only  $R \sim 1.3\text{Mpc}$  which MWA-5000 will not be able to observe.

#### 8. SCIENCE OPPORTUNITIES IN THE 21CM DETECTION OF INTERGALACTIC H II REGIONS

The results of the previous sections suggest some very interesting possibilities for science outcomes based on redshifted 21cm observations of H II regions. These lie in the

areas of the study of quasars and the unified model, in addition to study of the reionization itself.

Firstly, the detection of contrast between an H II region and a warm IGM offers a direct measure of the neutral fraction at that redshift. The serendipitous discovery of H II regions that will be feasible with the MWA-5000 (and possibly with the LFD) in addition to the study of H II regions around known high redshift quasars will allow a determination of the neutral fraction as a function of cosmic time. This will trace the evolution of neutral gas with redshift, providing the same information as the previously discussed global signature of reionization (Shaver et al. 1999). However the *observed* evolution from neutral to ionized IGM has a minimum width of  $\Delta z \sim 0.5$  due to a combination of cosmic variance and finite light travel time (Wyithe & Loeb 2004d). Since the global signature must therefore extend over more than one band-pass rather than occurring in a narrow step, it will be very difficult to calibrate. On the other hand, the interior of H II regions provide *built-in* calibrators at each redshift

where a measure of neutral fraction is made. Measurement of the evolution of neutral fraction with time using H II regions will be complimentary to measurements of the reionization history using the evolution in the power-spectrum of redshifted 21cm fluctuations (Furlanetto, Hernquist & Zaldarriaga 2004). The latter will provide a richer data set than observations of individual H II regions. However both types of measurement will be made using the same deep observations. They are complimentary since they will be subject to different systematic uncertainties.

Secondly, the observation of luminous quasar H II regions at a resolution that allows some detection of the geometry offer rich possibilities in AGN physics. For example, detection of the shape of the H II region will reveal the emission profile of the quasar. A conical region would imply that a dusty torus is present in these early quasars which obscures the ionizing emission. This phenomenon would be analogous to collimated outflows and ionization cones observed around low-redshift quasars. Detection of an asymmetry in the redshifts of the front and back of the H II region relative to the redshift of the quasar imply a relativistic expansion, and yield an estimate of the quasar lifetime (Wyithe & Loeb 2004b). The quasar lifetime could also be estimated from the duty-cycle. This quantity will be determined from the fraction of H II regions (with opening angles that include the line-of-sight for conical H II regions) that host active quasars. A direct measurement of the duty-cycle would yield important insight into the physics of the growth of early super-massive black holes.

In Figure 8 we showed that early in reionization, before clustering of sources becomes important in the generation of H II regions (Wyithe & Loeb 2004c; Furlanetto et al. 2004) H II regions larger than 2Mpc are generated by quasars which, while active, are detectable with Gemini in 200-300 seconds (with little sensitivity to redshift). Since there should be  $\sim 1$  such active quasar per field at  $z \sim 8$ , and  $\sim 100$  at  $z \sim 6$ , near-IR follow up of redshifted 21cm data may prove to be the most efficient means of discovering very high redshift quasars in the future, since only a hundred pointings per quasar will be required rather than a blind search of  $\sim 400$  square degrees. H II regions larger than 2Mpc (those that will be found by MWA-5000) will be dominated by quasars. However with the advent of SKA, H II regions smaller than 2Mpc in extent will be found. The detection of the lower luminosity quasars and luminous galaxies that generate these H II regions will require integration times of thousands of seconds per pointing for an 8m class telescope, quickly rendering searches of candidate H II regions for galaxies and quasars impractical. However the next generation of Extremely Large Telescopes (ELT) will provide the collecting area needed to perform the required integrations. For example the Giant Magellan Telescope would have an effective aperture

of greater than 20 square meters, and shorten the required integration time by nearly an order of magnitude (with additional improvement due to higher resolution imaging). This will allow discovery of lower luminosity sources that generate the smaller H II regions early in the reionization. Thus a combination of SKA and an ELT will allow us to follow the evolution of the topology of reionization and the sources that powered that evolution on a galaxy by galaxy basis.

## 9. CONCLUSION

In this paper we have assessed the sensitivity of three generations of planned low-frequency arrays, the LFD, MWA-5000 and SKA with respect to observing quasar generated H II regions. We find that an instrument of the class of the planned LFD will be able to obtain good signal to noise on H II regions around the most luminous quasars, and determine gross geometric properties in  $\sim 1000$  hours. The follow up MWA-5000 will be capable of mapping detailed geometry of H II regions, while SKA will be capable of detecting very narrow spectral features and will determine the sharpness of the H II region boundary. An SKA will most likely be limited by irreducible noise from fluctuations in the IGM itself. The MWA-5000 (and even the LFD in favorable circumstances) will discover serendipitous H II regions. We have estimated the number of such H II regions which are generated by quasars based on the observed number counts of quasars at  $z > 6$ , and find that there should be several-tens per field with radii larger than 4Mpc at  $z \sim 6 - 8$ . At redshifts where the IGM is predominantly neutral, large H II regions will be generated by quasars rather than by galaxies. Near-IR follow up of these H II regions with 8m class telescopes will be an efficient method for location of high redshift luminous quasars. Similarly, the smaller H II regions that will be identified by an SKA will provide sites to search for galaxies and low-luminosity quasars using the next generation of  $\sim 20 - 30$ m class telescopes, which will be sensitive enough to image normal galaxies and quasars in integrations of less than a thousand seconds. Detection of the massive host galaxies of dormant quasars could help reveal the impact of quasars on the evolution of galaxies. Thus, the study of H II regions, combined with targeted follow-up in the near-mid IR may provide the most efficient method for finding high redshift galaxies and quasars, and will in turn yield direct evidence for classes of sources responsible for reionization.

The authors would like to thank Miguel Morales for helpful comments on the manuscript. This work was supported in part by NASA grant NAG 5-13292, and by NSF grants AST-0071019, AST-0204514 (for A.L.). JSBW and DGB acknowledge the support of the Australian Research Council.

## REFERENCES

- Barkana, R., Loeb, A., 2003, *Nature*, 421, 341  
 ————. 2005a, *ApJ*, 624, L65  
 ————. 2005b, *ApJ*, submitted; astro-ph/0502083  
 ————. 2005c, *ApJ*, in press; astro-ph/0410129  
 Becker, R. H., et al. 2001, *AJ*, 122, 2850  
 Bertoldi, F., et al., 2003, *Astron. Astrophys. Lett.*, 409, L47  
 Cen, R. 2003, *ApJ*, 597, L13  
 Cen, R. 2003, *ApJ*, 591, L5  
 Cen, R., Haiman, Z., 2000, *ApJ*, 542, L74  
 Di Matteo, T., Perna, R., Abel, T., & Rees, M. J. 2002, *ApJ*, 564, 576

- Djorgovski, S. G., Castro, S., Stern, D., & Mahabal, A. A. 2001, ApJ, 560, L5
- Fan, X., et al. 2001 AJ, 122, 2833
- Fan, X., et al. 2001b, AJ, 121, 54
- . 2003, astro-ph/0301135
- . 2004, AJ, in press; astro-ph/0405138
- Furlanetto, S. R., & Briggs, F. H. 2004, New Astronomy Review, 48, 1039
- Furlanetto, S. R., Zaldarriaga, M., & Hernquist, L. 2004, ApJ, 613, 1
- Furlanetto, S.R. , Hernquist, L. & Zaldarriaga, M. 2004, MNRAS, submitted, astro-ph/0406131
- Furlanetto, S.R., & Loeb, A. 2005, ApJ, in press; astro-ph/0409656
- Gnedin, N. Y., & Shaver, P. A. 2004, ApJ, 608, 611
- Grimes, J. P., Kriss, G. A., & Espey, B. R. 1999, ApJ, 526, 130
- Gunn, J. E. & Peterson, B. A. 1965, ApJ, 142, 1633
- Iwamuro et al. 2004, astro-ph/0408517
- Kogut, A. et al. 2003, ApJ, submitted; astro-ph/0302213
- Kohler, K., Gnedin, N.Y., Miralda-Escude, J., Shaver, P.A. 2005, astro-ph/0501086
- Loeb, A., Barkana, R., Hernquist, L., 2005, ApJ, 620, 553
- Loeb, A., & Zaldarriaga, M. 2004, Phys. Rev. Lett., 91, 211301
- Madau, P., Rees, M.J., 2000, ApJ, 542, L69
- Maiolino et al. 2003, astro-ph/0312402
- Mesinger, A. & Haiman, Z. 2004, ApJ, submitted; astro-ph/0406188
- Morales, M. F., & Hewitt, J. 2004, ApJ, 615, 7
- Oh, S. P., & Mack, K. J. 2003, MNRAS, 346, 871
- Shaver, P. A., Windhorst, R. A., Madau, P., & de Bruyn, A. G. 1999, A&A, 345, 380
- Spergel, D. N., et al. 2003, AJ Supp., 148, 175
- Storchi-Bergmann, T., Wilson, A. S., & Baldwin, J. A. 1992, ApJ, 396, 45
- Tadhunter, C., & Tsvetanov, Z. 1989, Nature, 341, 422
- Tozzi, P., Madau, P., Meiksin, A., & Rees, M. J. 2000, ApJ, 528, 597
- Walter, F., et al., 2003, Nature, 424, 406
- Wang, X., Tegmark, M., Santos, M., , L., Knox, 2005, astro-ph/0501081
- White, R., Becker, R., Fan, X., Strauss, M. 2003, AJ, 126, 1
- Wyithe, J. S. B. & Loeb, A. 2002a, Nature, 417, 923
- 2002b, ApJ, 577, 57
- Wyithe, J. S. B. & Loeb, A., 2003a, ApJ, 588, 69
- Wyithe, J. S. B., & Loeb, A. 2003b, ApJ, 595, 614
- . 2004a, Nature, 427, 815
- . 2004b, ApJ, accepted, astro-ph/0401554
- . 2004c, ApJ, submitted, astro-ph/0407162
- . 2004d, Nature, in press, astro-ph/0409412
- Wyithe, J. S. B. & Loeb, A., Carilli, C., astro-ph/0411625
- Yu, Q. 2005, ApJ, 623, 683
- Zaldarriaga, M., Furlanetto, S. R., & Hernquist, L. 2004, ApJ, 608, 622